ISSN : 0974 - 7486 Volume 9 Issue 3

Trade Science Inc.

Materials Science

An Indian Journal

Full Paper

MSAIJ, 9(3), 2013 [113-118]

Correlation between structural and optical properties of SiO_2/TiO_2 multibilayers processed by sol-gel technique and applied to Bragg reflectors

H.Sedrati, R.Bensaha*, M.Brahimi, H.Dehdouh, H.Bensouyad, F.Abbas, B.Toubal
Laboratoire de Céramiques, Département de Physique, Université Constantine 1, Route Ain El-Bey, 25000 Constantine, (ALGÉRIA)
E-mail: bensaha@yahoo.fr

ABSTRACT

SiO_2 and TiO_2 thin layers processed by sol-gel technique have been deposited, alternatively, on glass substrates and Si (111) wafer. Dip-coated multibilayers were characterized by different experimental techniques: XRD, SEM, FTIR and UV-VIS-NIR. The obtained X-ray diffraction patterns analysis have shown that our films crystallize in anatase and rutile phases whatever is the number of bilayers and the corresponding grain sizes increase from 5.48 nm to 16.11 nm. The SEM micrograph shows that our layers are homogeneous without any visual cracks. The FTIR spectra have shown that the vibration of Si-O-Ti bonds becomes intense by the increase in the number of bilayers. This increase, on the on hand, decreases the transmission coefficient from 4.58% to 0.55% and increases the width of the stop band shown in UV-VIS-NIR spectra. On the other hand, the band-gap decreases from 3.73 eV to 3.59 eV. In addition, a pseudo band-gap is located between 300 nm and 400 increasing from 1.76 eV to 2.29 eV.

KEYWORDS

Sol-gel;
Anatase;
Rutile;
Stop band;
Si-O-Ti;
Band-gap.

INTRODUCTION

Because of its performance in developing thin films, facility to insert large quantities of optical transmitters in a matrix and low cost, the sol-gel method allows the development of materials at room temperatures from molecular precursors in a solution by series of chemical reactions[1].

Silicon oxide SiO_2 is a transparent dielectric material with a refractive index equals to 1.45 at 600-800 nm, which is already used to elaborate the multilayer which leads to a great interest in many important optical applications[2-7] namely in the industry due to its various properties: semiconductors, electronics and optoelectronics[8,11]. At 800 nm, TiO_2 possess refractive index equals to about 2.3. The significant uses of TiO_2 thin films are in solar cells[12,14], photo-catalytic systems[15] and electro-chromic systems[16].

Distributed Bragg reflectors are constituted of alternated high and low index quarter wave layers. To increase the reflection coefficient, the index contrast between the two materials and the number of layers have must be as high as possible[17,18]. It is thus natural to use SiO_2 and TiO_2 for the distributed Bragg reflectors[18].

The purpose of this paper is to study the effect of

Full Paper

the number of bilayers (the effective annealing time) on the optical and structural properties of SiO_2/TiO_2 multibilayers applied to Bragg reflector. For this, several experimental techniques were used to characterize structural and optical properties resulting from various numbers of bilayers (4, 6 and 8): X-ray diffraction, Scanning Electron Microscope (SEM), FTIR and UV-Vis spectroscopy.

EXPERIMENTS

Solutions preparation

SiO_2 sol

The SiO_2 sol was synthesized with Tetraethylorthosilicate (TEOS; $Si(OC_2H_5)_4$; 98.0% (GC), Fluka-Chemika). TEOS was mixed with Ethanol (Et; C_2H_5OH; 96% Reidel-de Haën) as solvent, ultrapure water (H_2O) for hydrolysis and few drops of hydrochloric acid (HCl; 37%) as catalyst. The obtained solution is very stable, homogeneous and clear.

TiO_2 sol

The TiO_2 sol was obtained after the dissolution of 1 mol of butanol (C_4H_9OH; 99.5%, Reidel-de Haën), 4 mol of acetic acid (CH_3COOH; 99-100%, Biochem-Chemopharma), 1 mol of distilled water and 1 mol of TetraButylOrthoTitanate (TBOT; $(C_4H_9O)_4Ti$; Fluka-Chemika). The final solution is Transparent of yellowish color[19,20].

Preparation of alternated thin layers procedure

As it is shown in Figure 1, the SiO_2 sol is deposited on a glass and silicon substrates as a bottom layer and after a heating/cooling operation we deposit the TiO_2 sol as a top layer forming one bilayer and so on till obtaining multibilayers. It is worth to mention that each deposited layer was dried at 100°C for 15 minutes then treated during one hour.

Preparation of samples

For this study, the various deposits were realized at the speed of dipping 7.69 cm.min^{-1}. We have prepared different number of bilayers (4, 6 and 8) and we have treated them at 500°C. The effective annealing time increases with the increase in the number of layer and, in the whole, it varies between 8 and 16 hours. Thus, increasing the number of bilayers corresponds to the increase in the annealing time.

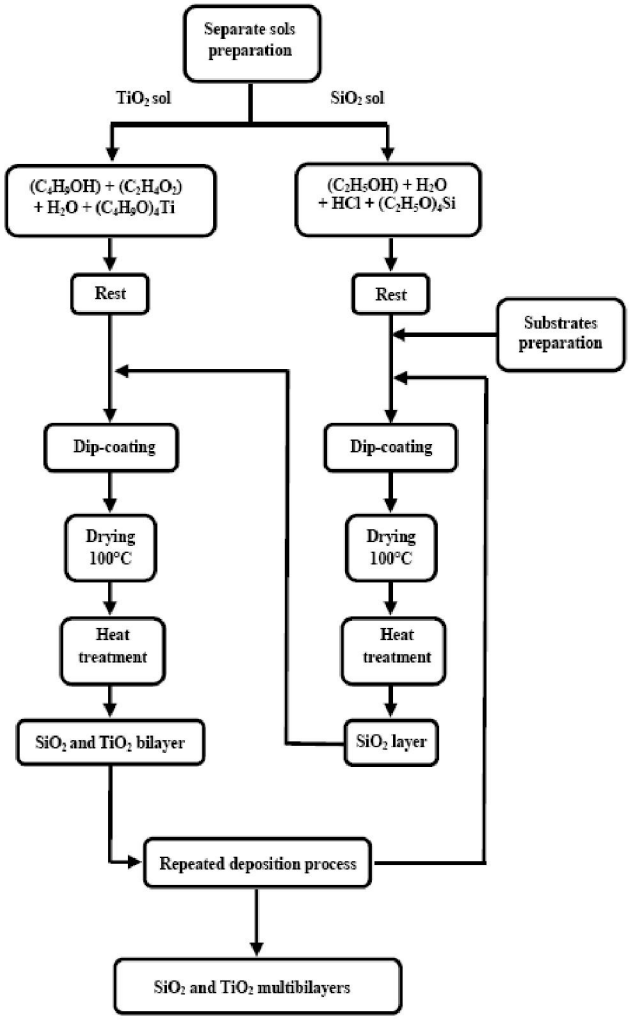

Figure 1 : Process of fabrication of SiO_2/TiO_2 multibilayers

Characterization techniques

X-ray diffraction was performed by "Bruker Axs Advanced" diffractometer using $CuK\alpha_1$ radiation (λ=1.5406 Å). The patterns were scanned at room temperature, over the angular range $0° < 2\theta < 95°$ with a step length of 0.05°/sec. The scanning Electron Microscopy (SEM) observations were obtained by using "JEOL JSM- 6360LV". Infrared spectra were performed using a spectrometer "Thermo-Nicolet Nexus 670", over the middle infra range (4000 - 400 cm^{-1}). The number of scanning is 32 with an estimated resolution of 4 cm^{-1} using a detector "DTGS KBr" and a splitter KBr. UV absorption studies were carried out using UV–VIS double-beam spectrophotometer.

RESULTS AND DISCUSSION

Structural properties

X-ray diffraction

Figure 2 displays the XRD patterns of SiO_2/TiO_2 multibilayers obtained at 500°C for 4 and 6 bilayers during 8 and 12 hours respectively. These diagrams show the variation of the crystal structure under the effect of the number of bilayers. The results show the presence of anatase and rutile phases of titanium oxide whatever is the number of bilayers.

On the one hand, Figure 2 (a) and 2 (b) show that the films crystalize in anatase phase corresponding to (101), (004), (200), (211)) and (204) plans respectively. On the other hand, Figure 2 (a) shows the presence of (211) plan corresponding to rutile phase. The last becomes important in the case of 6 bilayers which can be attributed to annealing time effect (Figure 2 (b)). This means that increasing the number of bilayers, or the annealing time, improves the crystallization phases[21].

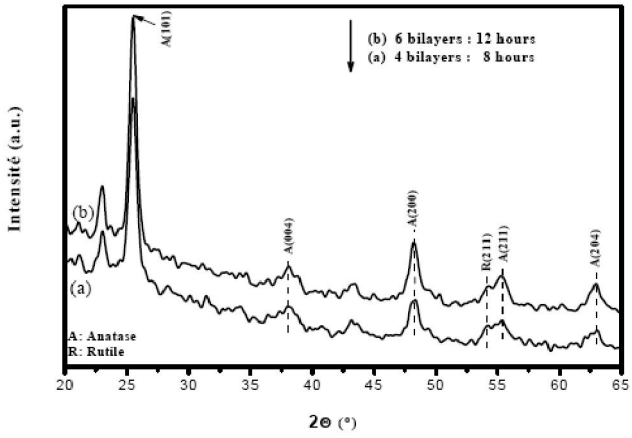

Figure 2 : Evolution of diffraction patterns of SiO_2 and TiO_2 multibilayers obtained at 500°C for: (a) 4 bilayers and (b) 6 bilayers during 8 and 12 hours respectively

Surface morphology and grain size

The crystallite size L of TiO_2 being in SiO_2/TiO_2 multibilayers can be deduced from XRD line broadening using Scherrer equation[22]:

$$D = \frac{0.94 \times \lambda}{\beta \cos\theta}$$

Where λ is the wavelength of X-ray beam (Cu Kα with λ=1.5406 Å), β is the full width at half maximum (FWHM) of (hkl) diffraction peak, and θ is the Bragg angle.

Using the size of the crystallites, the dislocation density (δ)[23], the number of crystallites/unit surface area (N) and strain in the films (ε) has been determined:

$$\delta = \frac{1}{D^2}$$

$$N = \frac{d}{D^3}$$

$$\varepsilon = \frac{\Delta(2\theta).\cos\theta}{4}$$

Where d is the film thickness.

The calculated structural parameters are presented in TABLE 1. The computed values of grain sizes, given in TABLE 1, were calculated for different number of bilayers with different annealing time. Thus, the obtained grain sizes of anatase and rutile increase from 5.48 nm to 16.11 nm and from 06.59 nm to 07.10 nm, respectively. In fact, as the number of bilayers increases the annealing time increases and the grain size also increases. It is interesting to note that the grain size improves and the defects like dislocation density and strain in the films decrease with film thickness. This may be due to the improvement in crystallinity in the films with film thickness.

Scanning electron microscope (SEM)

Figure 3 displays the SEM micrographs obtained for 8 bilayers treated at 500°C during 16 hours. It was observed that the coating was homogeneous without any visual cracks. So, the increase in the annealing time

TABLE 1 : Structural parameters of SiO_2/TiO_2 multibilayers

Number of Bilayers	Phase	D (nm)	(hkl)	δ (10^{-4}traits/nm^2)	N (10^{-3} nm^2)	ε (10^4)
4	Anatase	11.56	(101)	74.83	84.88	16.61
	Anatase	09.89	(004)	102.24	135.56	14.74
	Anatase	11.85	(200)	71.21	80.64	12.25
	Rutile	06.59	(211)	230.27	458.20	10,75
	Anatase	05.48	(211)	333.00	796,85	10,51
	Anatase	06.65	(204)	226.13	445,91	08,40
6	Anatase	12.35	(101)	65.56	125,35	15.54
	Anatase	16.11	(004)	38.53	56,47	13,55
	Anatase	12.08	(200)	68.53	133,94	11,47
	Rutile	07.10	(211)	198.37	659,71	10.04
	Anatase	06.73	(211)	220.78	774,62	09.82
	Anatase	09.59	(204)	108.73	267,73	07,85

Full Paper

did not affect the uniformity of the films.

Infrared spectrometry

To get the transmittance spectra by infrared spectrophotometry, we have realized the various deposits on Si (111) wafer. The FTIR spectra of SiO_2/TiO_2 multibilayers are presented in Figure 4. The last shows the infrared spectra between 2500 cm^{-1} and 400 cm^{-1} obtained for films sustained to 500°C during 8, 12 and 16 hours (Figure 4 (a), 4 (b) and 4 (c) respectively). These spectra show the presence of bands located between 443cm^{-1} and 1216 cm^{-1}. As we can see, a significant decrease of bonds located between 1093-1085 cm^{-1}, 813-809 cm^{-1}, 740- 736 cm^{-1}, 611-609 cm^{-1}, and 445-443 cm^{-1} that are assigned to the vibrations of Si-O-Si asymmetric stretching, Ti-OH, Si-O-Si symmetric stretching, Ti-O-Ti and O-Ti-O bonds respectively[24,25]. However, the band characteristic of Si-O-Ti bonds at around 960-950 cm^{-1} appears highly more intense as well as we increase the number of bilayers, indicating that the films with 8 bilayers present more Si-O-Ti bonds[26,27]. It is interesting to note, also, that bands observed around 445 cm^{-1} and 601 cm^{-1} are close to anatase and rutile phases, respectively[28].

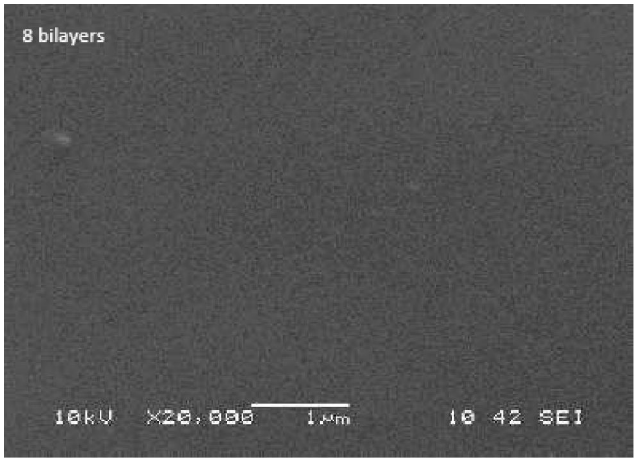

Figure 3 : SEM micrographs obtained at 500°C for 8 bilayers during 16 hours

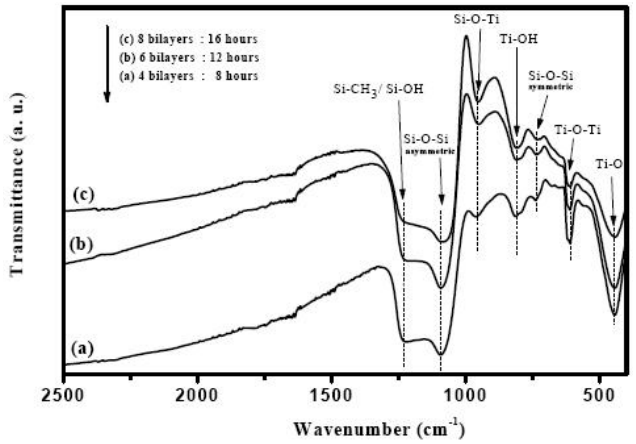

Figure 4 : IR Spectra of SiO_2/TiO_2 multibilayers for: (a) 4 bilayers, (b) 6 bilayers and (c) 8 bilayers during: 8, 12 and 16 hours respectively

Optical properties

UV absorption analysis

Figure 5 displays diffused scattering UV-VIS-NIR transmittance spectra of 4, 6 and 8 bilayers treated at 500°C in the spectral range 300-1200 nm. For more than 4 bilayers, the transmittance coefficient was of less than 1% in the spectral range (360-600nm) of the stop band. On the one hand, as the number of bilayers increases the transmission coefficient decreases from 4.58% to 0.55% and the stop band width increases from 157 nm to 168 nm (see TABLE 2). On the other hand, the wavy structure of the spectra at wavelengths exceeding 600 nm is due to interferences of waves that are not in the Bragg condition[29]. The occurrence of such waves means that our films are sufficiently thick[30]. A regular increase of the thickness with the number of bilayers is noticed (TABLE 2). As this number increases, a slight shift of transmission curves to higher wavelengths is observed. This shift is ascribed to the decrease in band-gap energy.

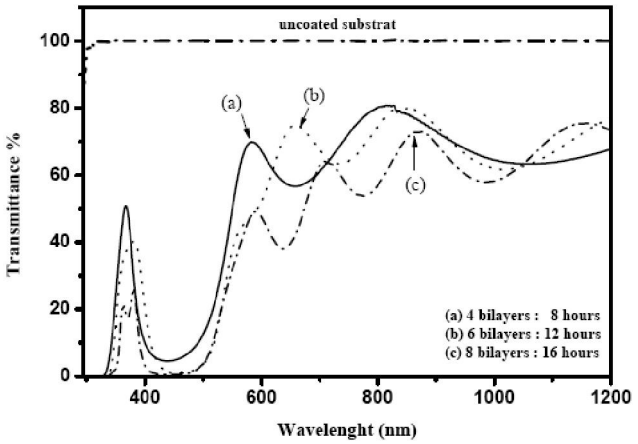

Figure 5 : UV-VIS spectra of SiO_2/TiO_2 multibilayers for: (a) 4 bilayers, (b) 6 bilayers and (c) 8 bilayers during: 8, 12 and 16 hours respectively

Refractive index and porosity

The refractive index of SiO_2/TiO_2 multibilayers was calculated from the measured UV-VIS-NIR transmit-

tance spectrum. The used evaluation method in this work is based on the UV-VIS-NIR transmittance spectrum analysis of a weakly absorbing film deposited on a non-absorbing substrate. The refractive index n(λ) over the spectral range is calculated by using the envelopes fitted to the measured extreme[31]:

$$n(\lambda) = \sqrt{S + \sqrt{S^2 - n_0^2(\lambda) n_S^2(\lambda)}}$$

$$S = \frac{1}{2}\left(n_0^2(\lambda) + n_S^2(\lambda)\right) + 2n_0 n_S \frac{T_{max}(\lambda) - T_{min}(\lambda)}{T_{max}(\lambda) \times T_{min}(\lambda)}$$

Where n_0 is the refractive index of air, ns is the refractive index of the film, T_{max} and T_{min} are the maximum and minimum envelopes respectively. The thickness of the films was adjusted to provide the best fits to the measured spectra. In this study, all the deposed films are assumed to be homogeneous. The porosity of the thin films is calculated using the following expression[32]:

$$\text{Porosite} = \left(1 - \frac{n^2 - 1}{n_d^2 - 1}\right) \times 100(\%)$$

Where n_d is the refractive index of pore-free anatase (n_d=2.52)[33], and n is refractive index of porous thin films.

The results of the computed refractive index (*n*), porosity (*p*) and thickness (*d*) are shown in TABLE 2. It is noted, on the one hand, that porosity and thickness increase with the increase in the number of bilayers from 0.283 to 0.491 and from 262.17 nm to 689.21 nm respectively. On the other hand, refractive index decreases from 2.20 to 1.93 since the thickness is inversely proportional to the index[29].

Energy band-gap

The band gap is then found as the intercept of the linear portion of the plot. For a direct band-gap semiconductor, the absorption near the band edge is given by Wang[34]:

TABLE 2 : Variation of refractive index (n), porosity (p), calculated film thickness and the stop band parameters of SiO_2/TiO_2 multibilayers obtained at 500°C

Number of bilayers	Effective annealing time (hours)	Réfractive Index	Porosity	Thickness	Stop band	
		n	P	d (nm)	T%	FWHM (nm)
4	8	2.20	0.283	262.17	4.58	157
6	12	2.06	0.397	472.24	0.98	161
8	16	1.93	0.491	689.21	0.55	168

$$(\alpha h\nu)^2 = C(h\nu - E_g)$$

Where C is a constant, E the optical band, α is the optical absorption coefficient, (hν) is the photon energy gap and h the Plank's constant.

The direct band-gap (E) of the films can be estimated by plotting (αhν) versus (hν) (Figure 6: (a), (b) and (c)), then extrapolating the straight-line part of the plot to the photon energy axis. The band-gap decreases owing to an increase in the number of bilayers. The values are 3.73 eV, 3.68 eV and 3.59 eV corresponding to 4, 6 and 8 bilayers respectively (Figure 6 (d)). This decrease can be correlated with grains size increases with effective annealing time, when the latter increases the defects and impurities tend to disappear causing a reorganization of the structure[30]. Moreover, a second band-gap is identified (pseudo band-gap) increasing from 1.76 eV to 2.29 eV with the increase in the number of bilayers (Figure 6 (d)). This pseudo band-gap is generated by the absorption band in the wavelength region located between 300 nm and 400 nm (see Figure 5).

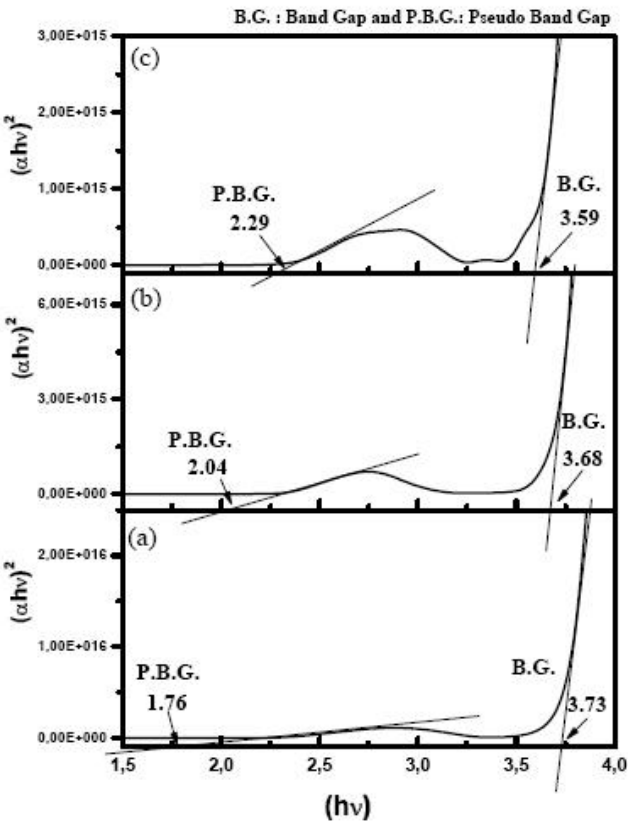

Figure 6 : Plot of (αhν) versus (hν) for determination of band gap of SiO_2/TiO_2 multibilayers for: (a) 4 bilayers, (b) 6 bilayers and (c) 8 bilayers during: 8, 12 and 16 hours respectively

Full Paper

CONCLUSION

In this study, optical and structural properties of SiO_2/TiO_2 multibilayers were studied using sol–gel technique. X-ray diffraction analyses show that the increase in the number of bilayers allow the formation of anatase and rutile phases. Calculation of grain sizes by Scherrer's formula, gives sizes ranging from 5.48 to 16.11 nm for all structures. The FTIR spectra show that Si-O-Ti bond vibration increases with the increase in the number of bilayers. UV-VIS-NIR transmission spectra show that increasing the number of bilayers the width of the stop band from 157 nm to 168 nm increases and the transmission coefficient decreases from 4.58% to 0.55% which can lead to a good Bragg reflector. The refractive index decreases with increasing number of bilayers, but the porosity decreases. The band-gap decreases from 3.73 eV to 3.59 eV and the pseudo band-gap increases from 1.76 eV to 2.29 eV owing to an increase in the number of bilayers.

REFERENCES

[1] C.J.Brinker, A.J.Hurd; J.Phys.III, France, **4**, 1231 **(1994)**.

[2] W.Geffcken, E.Berger; Deutches reichspatent 736411, assigned to Jenaer Glaswerk Schott & Gen., Jena, May 6 **(1939)**.

[3] E.M.Fishman, M.C.Abello, O.F.Gorriz, L.A.Arrùa; Applied Catalysis A: General, **319**, 111 **(2007)**.

[4] H.R.Phillip; Solid State Commun., **4**, 73 **(1966)**.

[5] D.L.Griscom; J.Non-Cryst.Solids, **24**, 155 **(1977)**.

[6] Y.N.Xu, W.Y.Ching; Phys.Rev.B, **44**, 11048 **(1991)**.

[7] Y.J.Kim, D.W.Shin; Journal of Ceramic Processing Research, **3(3)**, 186 **(2002)**.

[8] R.A.Higgins; Properties of Engineering Materials, ELBS, London, **(1985)**.

[9] M.Reyne; Les Matériaux Nouveaux, Hermes, Paris, **44**, **(1990)**.

[10] E.D.Palik; Handbook of optical constants of solids, Academic Press, Orlando, FL, **(1985)**.

[11] H.Raether; In: G.Holer (Ed); Springer tracts in modern physics, Springer-Verlag, Berlin, **88**, **(1980)**.

[12] S.A.Larson, J.L.Falconer; Appl.Catal.B: Environ., **4**, 149 **(1994)**.

[13] Y.Pas, A.Heller; J.Mater.Res., **12**, 2759 **(1997)**.

[14] K.Hara, T.Hariguchi, T.Kinoshita, K.Sayama, H.Arakawa; Solar Energy Mater.Solar Cell., **70**, 151 **(2001)**.

[15] V.A.Sakha, I.M.Arabatzis, I.K.Konstantinou, A.D.Dimou, T.A.Albanis, P.Falaras; Appl.Catal.B: Environ., **49**, 195 **(2004)**.

[16] Y.Tachibana, H.Ohsaki, A.Hayashi, A.Mitsui, Y.Hayashi; Vacuum, **59**, 836 **(2000)**.

[17] Y.G.Boucher, A.Chiasera, M.Ferrari, G.C.Righini; Optical Materials, **31**, 1306 **(2009)**.

[18] S.Rabaste, J.Bellessa, A.Broude, C.Bovier, J.C.Plenet, R.Brenier, O.Marty, J.Mugnier, J.Dumas; Thin Solid Films, **416**, 242 **(2002)**.

[19] R.Mechiakh, R.Bensaha, C.R.Physique; **7**, 464 **(2006)**.

[20] R.Mechiakh, F.Meriche, R.Kremer, R.Bensaha, B.Boudine, A.Boudrioua; Optical Material, **30**, 645 **(2007)**.

[21] G.Q.Liu, Z.G.Jin, T.Wang, Z.F.Liu; J.Sol-Gel Sci.Techn., **41**, 49 **(2007)**.

[22] B.D.Cullity; Elements of X-Ray Diffraction, 2nd Edition, Addison-Wesley, Reading, MA, 102 **(1978)**.

[23] S.Ray, R.Banerjee, A.K.Baraua; Jpn.J.Appl.Phys., **1889**, 19 **(1980)**.

[24] T.Oha, K.S.Ohb, K.Leec, C.K.Choib; Thin Solid Films, **468**, 316 **(2004)**.

[25] R.M.Almeida; J.Sol–Gel.Sci.Technol., **13**, 51 **(1998)**.

[26] M.Schraml-Marth, K.L.Walther, A.Wokan, B.E. Handy, A.Baiker, Journal of Non-Crystalline Solids, **143**, 93 **(1992)**.

[27] M.Aizawa, Y.Nosaka, N.Fujii, Journal of Non-Crystalline Solids, **168**, 49 **(1994)**.

[28] Jun-Ying Zhang, et al.; Journal of NonCrystalline Solids, **303**, 134 **(2002)**.

[29] M.Grün; Thesis Université H.Poincaré, Nancy, **1**, **(2010)**.

[30] H.Bensouyad, D.Adnane, H.Dehdouh, B.Toubal, M.Brahimi, H.Sedrati, R.Bensaha; J.Sol-Gel. Sci.Technol., **546–552**, 59 **(2011)**.

[31] J.C.Manifacier, J.Gasiot, J.P.Fillard; J.Phys.E, **9**, 1002 **(1976)**.

[32] B.E.Yoldas, P.W.Partlow; Thin Solid Films, **129**, 1 **(1985)**.

[33] W.D.Kingery, H.K.Bowen, D.R.Uhlmann; Introduction to Ceramics, Wiley, NY, **(1976)**.

[34] Y.L.Wang, K.Y.Zhang; Surûng Coat Technol, **140**, 155 **(2001)**.